Waterborne chitosan-epoxysilane hybrid pretreatments for corrosion protection of zinc

Christian Fernández-Solis[1] and Andreas Erbe[1,2]

[1)] *Max-Planck-Institut für Eisenforschung GmbH, Department of Interface Chemistry and Surface Engineering, Max-Planck-Str. 1, 40237 Düsseldorf, Germany*

[2)] *NTNU - Norwegian University of Science and Technology, Department of Materials Science and Engineering, 7491 Trondheim, Norway*[a)]

(Dated: 10 March 2016)

Biopolymer-based systems are extensively studied as green alternatives for traditional polymer coatings, e.g. in corrosion protection. Chitosan-epoxysilane hybrid films are presented in this work as a chitosan-based protective system, which could e.g. be applied in a pretreatment step. For the preparation of the chitosan-epoxysilane hybrid systems, a sol-gel procedure was applied. The function of the silane is to ensure adhesion to the substrate. On zinc substrates, homogeneous thin films with thickness of $50 - 70$ nm were obtained after thermal curing. The hybrid-coated zinc substrates were characterized by infrared (IR) spectroscopy, ellipsometry and X-ray photoelectron spectroscopy (XPS). As model corrosion experiments, linear polarization resistance was measured, and cathodic delamination of the weak polymer coating poly(vinylbutyral) [PVB] was studied using scanning Kelvin probe. Overall, chitosan-epoxysilane hybrid pretreated samples showed lower delamination rates than unmodified chitosan coatings and pure PVB. Electrochemical impedance spectroscopy (EIS) confirmed a reduced ion permeability and water uptake by chitosan-epoxysilane films compared to that of a non-modified chitosan coating. Even though the coatings are hydrophobic and contain water, they slow down cathodic delamination by limiting ion transport.

[a)] Electronic mail: aerbe@arcor.de, a.erbe@mpie.de

I. INTRODUCTION

Corrosion of metallic materials is one of the most relevant natural occurring phenomena and has an important economic impact.[1] Polymer coatings present a simple and hence popular form of passive protection of metallic surfaces.[2] Hence, polymer coatings in their role of protecting metal against corrosion have been studied extensively.[3–6] Recently, efforts on reducing the emission of volatile organic compounds (VOC) are increasing, in line with world wide legislation changes. Therefore, studies focusing on the use of more environmentally friendly materials have significantly increased. Research activity has also been focused on the utilization of materials present in large quantities in nature which can be easily extracted, e.g. from industrial wastes.[7–9]

Polysaccharides such as chitin, cellulose, and starch possess are highly available and become interesting candidates for new formulation of coatings. Chitin is one of the most abundant polysaccharides on earth, only being surpassed by cellulose.[10–12] It is the main structural component of many organisms such crustaceans exoskeletons, insects, arthropods and some species of algae.[13–15] Since chitin is insoluble in almost all known solvents, its utilization has encountered many limitations. However, chitosan, its de-acetylated derivative, is soluble in aqueous acidic media.

Therefore, several recent studies focus on chitosan as a waterborne environmentally friendly protective alternative for coatings with diverse applications.[16–19] Chitosan has applications in numerous fields such cosmetics, water treatment, food processing and coatings, because of to its ability to bind a variety of molecules, its antimicrobial activity, its biodegradability and its excellent film forming ability.[7,20–25] Even though chitosan shows high adhesion to metallic surfaces and good film-forming properties, its high permeability to water imposes limitations in applicability.[26] Nevertheless, several modifications on the hydroxyl and amino groups of the glucosamine units of chitosan have been reported to yield derivatives with improved properties for corrosion protection of aluminium alloys.[18,19]

In recent years, several studies have reported the preparation of films using polysaccharides and chitosan as matrix.[27–32] Chitosan-silane hybrids have been shown to exhibit biocompatibility for proliferation of osteoblastic cell lines: cells cultured on chitosan-silane hybrids exhibited increased alkaline phosphatase activity compared to cells cultured on unmodified chitosan membranes.[27] Additionally, there are attempts to combine chitosan with

minerals to obtain composites for applications in tissues engineering, due to the ability of chitosan to complex calcium cations and to form porous films that permit migration of cells into the film.[25] Moreover, chitosan degrades into non-toxic compounds.[25] Chitosan and its derivatives have also been used in several environmental applications. Chitosan selectively binds certain cations, which permits sorption of metal traces. Moreover, it has been used for remediation of organic contaminants and immobilization of enzymes containing systems and stabilization of nanoparticles.[33]

This work explores the ability to form biocompatible coatings that may be used to protect metals in contact with biological environment against corrosion. We address the preparation of a chitosan-based film, using sol-gel chemistry, to produce chitosan-epoxysilane hybrid films deposited on metallic zinc. We investigate the formation of a hybrid coating by cross-linking chitosan in solution with a water-soluble epoxysilane coupling agent. The sol-gel chemistry should enable the production of a hybrid film by controlling the temperature and pH. Epoxy-silane coupling agents have been reported for numerous application in metal protection, because of thermal resistance and capability of cross-linking amine and hydroxyl groups.[34]

Zinc was used as a model for galvanized steel, which is frequently coated with polymer coatings.[5,35,36] Cathodic delamination starting on an electrolyte-filled defect is one of the main mechanisms of de-adhesion of coatings from galvanized products.[35–38] In cathodic delamination, a delamination front headed by a region of oxygen reduction and followed by a region of metal dissolution propagates at the coating/metal interface.[38–41] Silanes covalently bound to the interface can significantly slow down delamination.[42] Ion migration to balance the electronic current through the solid is an important part of the mechanism.[43–45] The presence of water in the interfacial region is critical for ion migration to occur. Typically, organic coatings are hydrophobic barriers.[5,35,36] Hydrophobicity, however, generates a chemical potential gradient in the vicinity of a defect, hence a driving force for water transport into the coating. Using coatings which can absorb large fractions of water, such as chitosan, removes this gradient. An investigation of the effects of the presence of water in the interfacial region on the delamination is the main motivation of this work. Recently, water consumption was suggested to be responsible for the observation of oscillations in the delamination process.[46]

The aim is to use water soluble chitosan as the main structural component of a pre-

treatment-like film, enhancing its stability by the presence of intra- and intermolecular organosiloxane bounding. Chitosan and chitosan-epoxysilane were characterized using infrared reflectance absorbance spectroscopy (IRRAS), ellipsometric spectroscopy and X-ray photoelectron spectroscopy (XPS). Corrosion inhibition properties, water uptake, ion permeability and delamination kinetics were studied by electrochemical impedance spectroscopy (EIS), linear polarization resistance (LPR) and scanning Kelvin probe (SKP) experiments.

II. EXPERIMENTAL SECTION

A. Materials

Zinc sheets (purity, 99.95%) with a thickness of 1.5 mm were supplied by Goodfellow (Cambridge, UK). Chitosan (weight-averaged molecular weight 650000 g mol^{-1}, min. 80% deacetylated) was obtained from Wako Pure Chemical Industries (Osaka, Japan). The epoxysilane coupling agent 2-(3,4-epoxycyclohexyl)ethyiltrimethoxysilane (97%) was obtained from ABCR (Karlsruhe, Germany). All chemicals were used as received unless otherwise noted. Zinc substrates (15 mm×15 mm) were mechanically ground with SiC paper up to 4000 grit and subsequently polished with an oxide polishing suspension (SiO_2, diameter 50 nm) to smooth the surface. Polished samples were ultrasonicated in acetone and dried in a nitrogen stream.

B. Preparation of coatings

Chitosan solution was prepared by adding chitosan flakes (1 g) to 100 mL of diluted acetic acid (0.2 M) and stirring over night at 50°C. Afterwards, the solution was cooled down to room temperature and kept in a glass bottle, protected from light. Since the flakes were completely dissolved after this procedure, no filtration prior to use was required.

For preparation of the chitosan-epoxysilane hybrid coating, 15 µL of 2-(3,4-epoxycyclohexyl)ethyl-trimethoxy-silane (97%) were added to 1 mL of chitosan solution and sonicated for 1 min. The mixture was spin-coated onto zinc at 55 rpm for 30 s, and the obtained film subsequently cured at 100°C for 2 h.

For each experiment, an unmodified chitosan solution (i.e., without epoxysilane) was also applied on a separate zinc sample and used for comparison.

C. Characterization methods

Samples were characterized by IRRAS on a Bruker Vertex 70v Fourier transform IR spectrometer (Bruker, Karlsruhe, Germany) equipped with a nitrogen cooled middle band mercury cadmium telluride detector. IR spectra were recorded with a spectral resolution of 4 cm^{-1} at an incidence angle of 80° using p-polarized light. Spectra shown in this work were recorded using a background of the corresponding freshly cleaned zinc sample without coating. For each spectrum, 250 scans were averaged.

Thickness of the layers was determined by ellipsometry. Measurements were performed using a UV/visible spectroscopic ellipsometer (SE 800, Sentech Instruments, Berlin / Krailling, Germany) in the wavelength range of 400 to 800 nm at an angle of incidence of 70°. Film thickness was obtained after averaging measurements at three different spots per sample, modelling with a simple ambient-layer-substrate model and fixing the refractive index of the polymer coating wavelength-independent to 1.52.[47] Differences in the ellipsometric parameters were analysed with respect to the bare zinc substrate for each sample. Using this procedure, differences in the formed zinc oxide layer on the samples will affect the determined thickness.

The surface composition was analyzed by XPS (Quantera 2, Physical Electronics, Chanhassen, MN, USA) with a monochromatic Al Kα source (1486.6 eV) at a pass energy of 26 eV and with energy step of 0.1 eV. Survey scans were performed to scan the sample for relevant elements (pass energy = 140 eV, energy step = 0.5 eV). The take-off angle was 45°. The binding energy scale was referenced to the C-C signal at 284.8 eV binding energy. Sputter depth profiling was performed with an energy of 2 keV with a raster area of 2 mm^2. Sputtering time per cycle was 1 min, corresponding to $\approx$ 7.5 nm/min. The sputtering rate was determined dividing the thickness of the film obtained from ellipsometric measurements by the total time necessary to sputter through the film, which was monitored by the sputtering profile. The total time was used until the C 1s peak reached the noise level.

D. Cathodic delamination experiments

Delamination experiments were performed on a commercial SKP system KM Soft Control (Wicinski - Wicinski GbR, Wuppertal, Germany) equipped with a 100 µm diameter NiCr tip

in a humidity chamber with relative humidity of ≈95% at room temperature. Proceeding each experiment, the SKP was calibrated to the standard hydrogen electrode (SHE) against Cu|saturated $CuSO_4$ solution.[41]

For delamination studies, spreading of electrolyte over the sample surface was avoided by spin coating each sample with a 5 % alcoholic solution of poly(vinyl butyral) [PVB], to yield a top coating of ≈1 μm thickness. As control experiment, bare zinc substrates were spin coated with PVB and delamination experiments were performed under same conditions. For initiation of the cathodic delamination process, an artificial defect was created at the edge and filled with 1M KCl. Progress of the delamination front was analysed as described elsewhere.[41] The first point exhibiting the potential of the intact interface was taken as the position of the delamination front.

E. Electrochemical characterization

Electrochemical experiments were performed using a Compactstat potentiostat (Ivium Technologies, Eindhoven, The Netherlands), in a three electrode geometry with a self-made cell. As counter electrode, a gold foil was used. A commercial Ag|AgCl|3M KCl reference electrode (Metrohm, Filderstadt, Germany) served as reference electrode. All tested samples had a geometric area of 0.196 cm^2 and no additional PVB was top-coated on the samples.

LPR experiments were executed in 0.1M KCl electrolyte at a scan rate of 1 mVs^{-1}. The potentiodynamic measurements were started after 1 h of stabilization of the open circuit potential (OCP). Polarisation was carried out starting with cathodic polarization at −150 mV with respect to OCP, followed by polarising to +150 mV in anodic direction from OCP. Corrosion current densities i_{corr} were calculated from the polarization resistance R_p according to a procedure explained elsewhere.[48] R_p was determined as the slope of the linear polarization curve from ±15 mV around E_{corr}. The Tafel slopes of the anodic and cathodic branch, β_a and β_c, respectively, were obtained from linear regions of the Tafel plots. Corrosion current densities were then calculated as[48]

$$i_{corr} = \frac{\beta_a \beta_c}{\ln(10) R_p (\beta_a + \beta_c)} \tag{1}$$

EIS was performed to evaluate the barrier properties of chitosan and silane-chitosan coatings against corrosion of zinc substrates. EIS was performed in the frequency range of 0.001 to

1000 Hz with 10 mV of sinusoidal perturbation around the OCP, measuring at 4 frequencies per decade. The total number of frequencies was kept low to ensure a fast measurement and to avoid subsequent interpretation problems arising from a system that changes significantly during measurement. The experiments were conducted in a borate buffered sulfate, prepared from 0.2M H_3BO_3, 0.05M $Na_2B_4O_7$, and 0.1M Na_2SO_4. The pH of the solution was measured as 8.2 ± 0.3. This electrolyte provides good conductivity to perform EIS experiments and suppresses undesired formation of corrosion products. Obtained data were modelled using the programme EISfit[49] by fitting to equivalent circuits which have been shown to describe well a polymer|oxide|metal system.[36,38,50] No constant phase elements were used for fitting.

The capacitances of chitosan and chitosan-epoxysilane layers C_c obtained from the fitted data were used to extract the uptake of water. For classical hydrophobic coatings, water content in coatings represents a factor of degradation of the system's protective properties, and consequent undercoating corrosion. Therefore water uptake has been substantially studied.[51–54] The variation of coating capacitance C_c with the amount of water is typically expressed as applicable for a plate capacitor[51,53,55]

$$C_c = \epsilon\epsilon_0 \frac{A}{d}, \tag{2}$$

where ϵ is the relative dielectric constant of the coating, ϵ_0 dielectric constant of vacuum, A the area of the sample and d the thickness of the coating. Normally, the dielectric constant of water is much higher than that of polymers, thereby the general increase of the coatings dielectric constant ϵ is due to incorporation of water.

Brasher and Kingsbury have proposed an effective equation for the estimation of water volume fraction ϕ in an organic coating[51]

$$\phi(t) = K \frac{\log_{10}(C(t)/C_0)}{\log_{10} \epsilon_W} \tag{3}$$

where K is measure of the swelling of the coating layer, $C(t)$ is the capacitance of the polymer at time t, C_0 is the initial capacitance of the coating and ϵ_W is the dielectric constant of water. Because the coating system investigated here may contain water from the beginning, estimates of C_0 were required. (C_0 is in this work interpreted as the initial capacitance of the coating, not as the capacitance with the coating without water.) Such estimates were obtained by extrapolating $C(t)$ to $t = 0$. The value of ϵ_W was considered 80 at room temperature. The effect of increasing thickness of the polymeric layer was neglected

($K = 1$). Because water may be present in the coatings from the beginning, the resulting ϕ presents the fraction of water taken up in the swelling process, which is a lower estimate for the total water volume fraction.

III. RESULTS AND DISCUSSION

A. Preparation of chitosan-epoxysilane mixed coatings

An schematic representation of the chemical processes possible during deposition of the chitosan-epoxysilane hybrid films are shown in Figure 1. The silane coupling agent used to obtain the chitosan-epoxysilane coatings is a water soluble epoxy-silane. Epoxy-silanes are capable of cross-linking, mainly, the amine and hydroxyl groups present in the chitosan molecules. Chitosan-epoxysilane hybrids with controllable thickness obtained using similar methods have been reported.[27,28,56] The aqueous solution of chitosan facilitates the hydrolysis of silane groups. The acidic medium facilitates the activation of the epoxy group and the positively charged ammonium groups enhance interaction with the epoxysilane hydroxyl groups. The concentration of epoxy-silane was kept under 1.5 wt% to minimize inter-silane condensation.[57] The deposited coating was thermally cured at 100°C to ensure total activation of the epoxy functional group as well as to facilitate formation of siloxane bonds.

B. Characterization of chitosan layers

The thickness of the prepared coatings was determined by ellipsometry as 60 ± 14 nm. To examine the composition of the chitosan-epoxysilane hybrid coatings, IRRA and XP spectra were recorded. Figure 2 shows the IR spectra of a chitosan coating (Figure 2a) and a chitosan-epoxysilane hybrid (Figure 2b) on zinc. Characteristic peaks corresponding to chitosan were in general shifted to lower wavenumbers for the chitosan-epoxysilane hybrid system. Peaks have been assigned on empirical basis.[27,58–60] The broad band between 3750 and 3000 cm^{-1} arises from overlapping ν(OH) and ν(NH) modes. The peak at 2931 cm^{-1} is assigned to a ν(C-H) mode. The bands corresponding to the characteristic amide I and II modes of chitosan were observed at 1662 $cm^{-1}$and 1595 $cm^{-1}$for chitosan, respectively, while they were shifted to 1658 cm^{-1} and 1558 cm^{-1} for the hybrid system. Additionally,

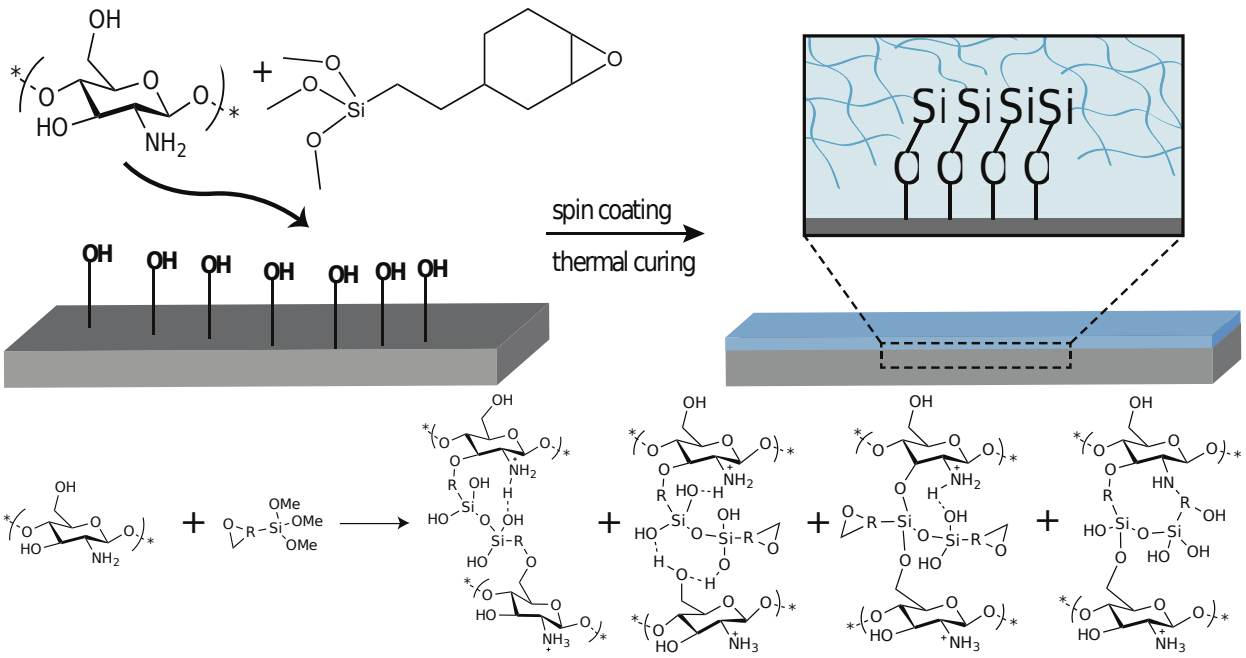

FIG. 1. Scheme of coating formation with chemical structure of chitosan, the employed epoxysilane coupling agent and possible reaction paths during coating formation.

in the chitosan-epoxysilane hybrid, a peak at 1726 cm^{-1} arises, indicating the formation of an ester bond.[58] The presence of this peak indicates cross-linking of hydroxyl and amines groups of chitosan with the epoxysilane coupling agent. The peaks at 1441 cm^{-1}, 1254 cm^{-1} and 1071 cm^{-1} are the stretching vibrations corresponding to C-O-C of the polysaccharide structure. The small peak at 1335 cm^{-1} corresponds to a CH bending mode. Furthermore, characteristic peaks of organosiloxanes were observed at 1374 cm^{-1}, 1190 cm^{-1}, 898 cm^{-1} and 810 cm^{-1}, corresponding to Si-O-Si and Si-C vibrations.[27,60]

In the XP spectra (Figure 3a), Zn peaks were absent on the surface of coated samples, indicating a homogeneous coverage of substrate with the hybrid coating. Si 2s and 2p peaks were observed, indicating the presence of siloxane bonds.[61,62] Both Si 2p and O 1s peaks were observed throughout the whole depth profile. After several sputtering cycles, C and N signals corresponding to the chitosan component were absent, while the Si 2p and O 1s peaks remained centred at 102 eV and ≈532 eV, respectively, as shown in Figure 3. Consequently, the epoxysilanes formed a layer on the substrate surface which connected the organic chitosan to the zinc.

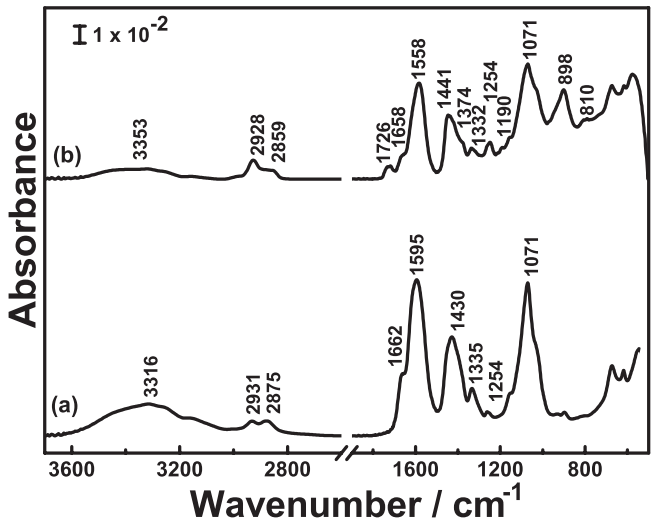

FIG. 2. IRRA spectra of (a) chitosan coatings and (b) chitosan-epoxysilane hybrid coatings on zinc. Spectra have been vertically offset for clarity.

C. Electrochemical properties of the coatings

In order to study the stability of the chitosan-epoxysilane hybrid coatings, cathodic delamination experiments were performed by SKP. Figure 4a shows the SKP potential profile of the propagation of a delamination front from an artificial defect filled with 1M KCl for a sample coated with chitosan-epoxysilane and top coated with PVB. Figure 4b shows the SKP potential profile of a PVB coated sample, used a reference. The profiles were obtained by scanning along the surface from the generated defect as explained in the experimental section. The recorded potentials were plotted as function of distance from the defect for different intervals of time. The potential at the interface recorded during the first hours of the experiment was ≈ 0 V vs. SHE, the potential of an intact interface, with no corrosion processes taking place.[41] The high humidity in the chamber and the electrolyte in the defect will eventually lead to initiation of cathodic delamination. On PVB, in this case the potential corresponding to freely corroding zinc was observed (≈ -0.7 V vs. SHE). However, for chitosan-epoxysilane films, this potential was not reached during the experiment. Instead, a potential of ≈ -0.5 to ≈ -0.3 V vs. SHE was observed. Nevertheless, a propagation front with a potential drop of ≈ 400 mV was recorded, similar to the case of PVB, and a velocity of the progress of the front was calculated. The offset in the potential value observed in Figure 4a could be attributed to effects of Donnan potentials, as results of the semi-permeable

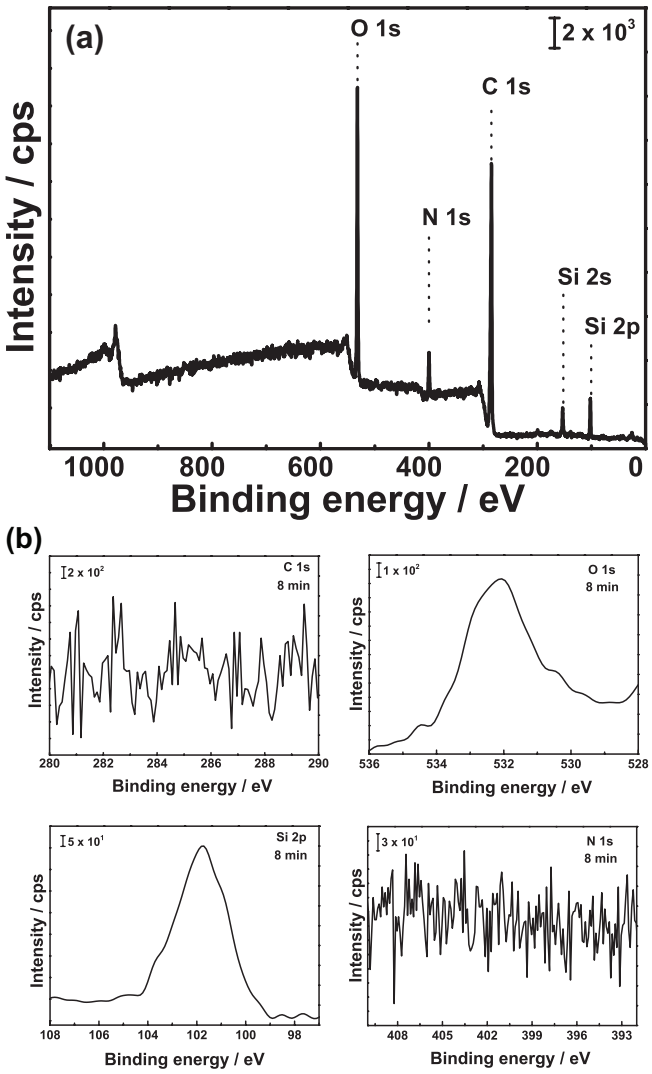

FIG. 3. XPS spectra for (a) survey at the coating interface and (b) after 8 min (corresponding to 60 nm) of argon sputtering, near the film/metal interface.

membrane behavior of the chitosan-epoxysilane hybrid.

The progress of the delamination front with time t is displayed in Figure 5a for chitosan and chitosan-epoxysilane hybrid films. Figure 5b shows the same results plotted on a double logarithmic scale, which facilitates the determination of the exponent α of the time dependence. A diffusion controlled process shows a delamination front that travels as $d \propto t^{1/2}$ ($\alpha = 1/2$).[63] A time dependence of $d \propto t^1$ ($\alpha = 1$) is expected either if a first-order reaction is rate-determining or for short-distance ionic migration.[42,63] During the first stage of the delamination of the chitosan-epoxysilane coating, a linear time dependence was observed. Consequently, delamination in this system is not diffusion-controlled, rather the rate may be

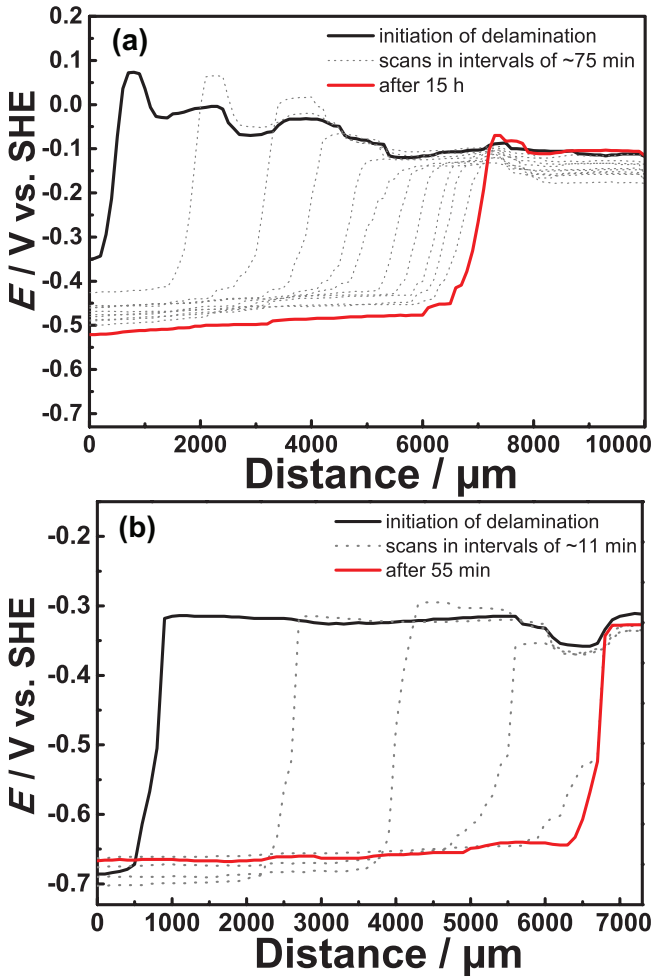

FIG. 4. SKP delamination profile of (a) chitosan-epoxysilane hybrid coating on zinc top coated with PVB and (b) PVB coated zinc use as reference, both at relative humidity of ≈95%. The defect is in contact with 1M KCl.

controlled by a short distance migration of ions.[63] For all systems, the initial delamination rate r was determined from the initial slope of a linear fit in Figure 5a. Delamination rates for the coatings are presented in Table I.

Compared to the reference of PVB coated substrates, the initial delamination rate of chitosan coated zinc decreased to 1/5. For the reference system, the delamination rate found here is comparable to the rate found in our lab in previous works.[42] Chitosan-epoxysilane films showed a delamination rate of 0.24 ± 0.02 mm h^{-1}, therefore representing the highest inhibition of delamination found in this work. The delamination rate of chitosan-epoxysilane hybrid coatings is comparable to those of covalently bound coatings.[42]

The long-time delamination curves of chitosan-epoxysilane hybrid exhibit a non-linear

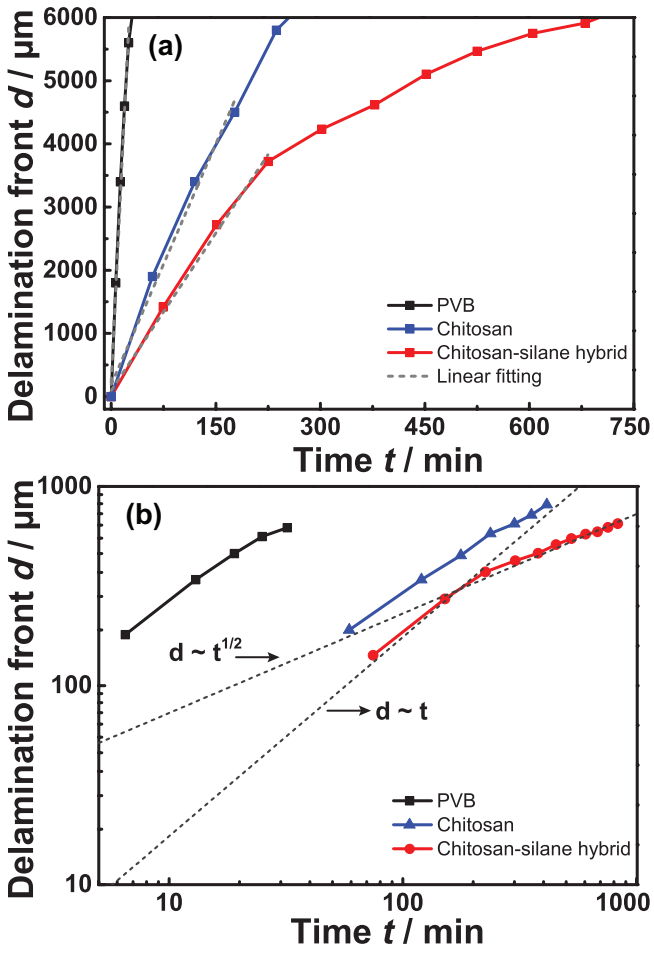

FIG. 5. Progress of the delamination front for different samples (a) on linear scale and (b) on a double logarithmic scale. In (a), linear fits of the initial slopes are indicated as dashed lines. In (b), dotted lines show the expected slopes for $d \propto t$ and $d \propto t^{1/2}$, as indicated in the graph. A PVB top coat was present on all samples, see section II.

progress. A linear fit of the data in Figure 5b enables a determination of the exponent α characterising the time dependence. Fitting the long-time delamination curves of the chitosan-epoxysilane hybrid to this expression, an exponent $\alpha = 0.46 \pm 0.01$ was obtained. This α value is very close to diffusion controlled processes, where the delamination front propagates at a rate $d \approx t^{1/2}$.[42,44,63] On the other hand, the α corresponding to unmodified chitosan and PVB are 0.70 ± 0.03 and 0.81 ± 0.04, respectively. The value for PVB is lowered by edge effects in the last data point, which was close to full delamination of the sample. Notice that for the chitosan-epoxsilane hybrid coating, the characteristic time dependence changed in the course of the experiment. Figure 5b shows that for small times, the system

TABLE I. Delamination rates and their standard deviations for different samples. All samples were top coated with PVB, see section II

sample	delamination rate / mm h^{-1}
PVB	11 ± 1
chitosan	2.0 ± 0.3
chitosan-epoxysilane	0.24 ± 0.02

behaves close to $d \approx t^1$, while a cross-over was observed to diffusion-limited behaviour, $d \approx t^{1/2}$. The rate determining step for the delamination of chitosan-epoxysilane coatings after long times was most likely ion transport through the film (see below), but may also be oxygen transport.

Even though a delamination front propagates with time, the potential of freely corroding zinc was not reached for the chitosan-epoxysilane system. This observation suggests that little of the electrolyte gets in direct contact with the oxide-covered metal interface, rather a part of the ions were selectively retained within the chitosan-epoxysilane matrix. Therefore, in the first stage of the delamination, a high amount of ions from the electrolyte were probably penetrating the film. However, with time the electrolyte concentration approached saturation, slowing down the progress of the delamination front, as shown in Figure 5a. The main driving force for the progress of the delamination front is the oxygen reduction. However, a flow of ions is needed to balance the electron flow through the solid.[38] Chitosan cross-linked films have been reported to inhibit ion diffusion.[64] Even though cross-linked chitosan films are permeable to K^+ ions, it is likely that Zn^{2+} that were formed in the beginning of the delamination have a lower diffusion coefficient[64] through the film. Hence, they were retained at intact interface of film. As a result, a "blocking net" is formed, with an electric field gradient, consequently restricting the migration of K^+. Therefore, we attribute the observed long-term diffusion control to ion transport. In this picture, the observed cross-over from $\alpha = 1$ to $\alpha = 0.5$ is from a regime where ion migration in the electric field gradient is rate determining, to a regime where ion diffusion is the rate controlling step.

Linear polarization experiments were used to evaluate the electrochemical behaviour of the films in aqueous solution. Typical Tafel plots obtained for bare zinc and coated zinc are shown in Figure 6. Quantitative analysis of polarisation curves is in general only possible

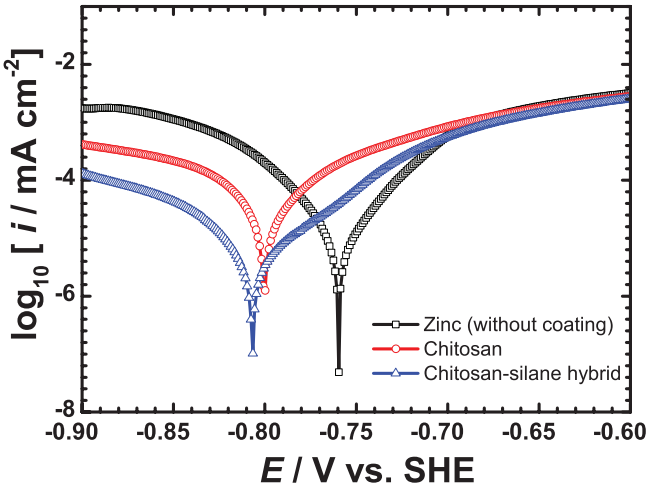

FIG. 6. Tafel plots of polarization curves for zinc, chitosan, and chitosan-epoxysilane coated zinc in 0.1M KCl.

if the curves follow the exponential dependence of currents on the potential in a certain region around the OCP.[65] As the chitosan-based coatings are swollen, electrolyte is present in the vicinity of the metal surface. Hence, electron transfer reactions can occur at the metal/electrolyte interface, and a piecewise linear Tafel plot of the coated samples is expected. Figure 6 shows that for the coated samples, linear regions were actually obtained in the Tafel plot, which justifies a further quantification. Extracted corrosion current densities calculated from the polarization resistance are tabulated in Table II. Certainly, the corrosion current density of bare zinc represents the highest value in this series. The chitosan-epoxysilane coating exhibited much lower corrosion current density. From the Tafel plots in Figure 6 it is obvious that the cathodic branch, including the oxygen reduction current, was strongly inhibited by the chitosane-epoxysilane coating. On the anodic side, representing metal dissolution, current densities for both coatings reached the values of the bare zinc at large potentials above the OCP. However, the chitosan-epoxysilane coatings significantly reduced anodic current densities at low positive potential differences to the OCP.

D. Time-dependent barrier properties and ion permeability evaluated by EIS

The water uptake and stability of the produced coatings were assessed by time-dependent EIS. Figure 7a shows area-normalized impedance spectra for both coatings on zinc after 2 h of immersion in borate buffer. EIS data of chitosan-epoxysilane films were fitted to the

TABLE II. Corrosion current densities i_{corr} and other parameters extracted from linear polarisation measurements for different samples in 0.1M KCl

sample	β_a/ mV dec^{-1}	β_c / mV dec^{-1}	R_p / Ω cm^2	i_{corr} / μA cm^{-2}
zinc uncoated	144 ± 6	181 ± 5	316 ± 14	110 ± 10
chitosan	120 ± 5	171 ± 5	825 ± 50	37 ± 4
chitosan-epoxysilane	66 ± 4	115 ± 5	3830 ± 150	4.8 ± 0.4

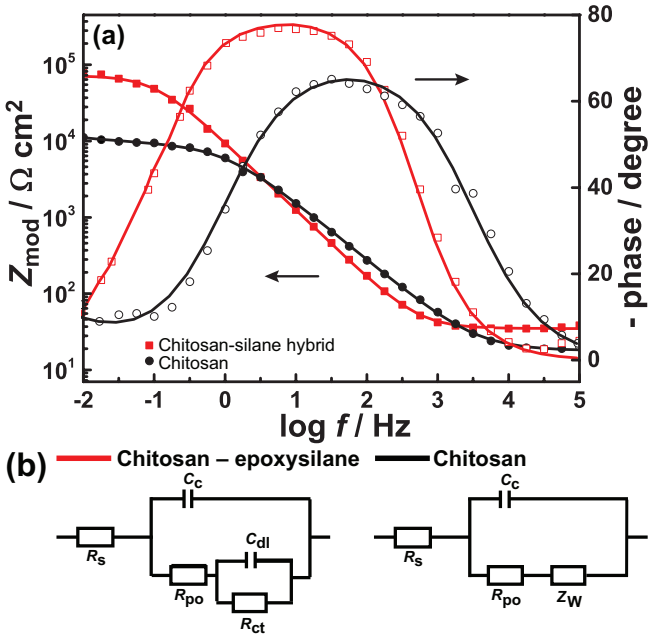

FIG. 7. (a) Bode plots after 2 h of immersion in borate buffer (points - measured data, lines - fit), (b) equivalent circuits used to fit EIS measurements. Left circuit: chitosan-epoxysilane coating, right circuit: chitosan coating. R_s is the solution resistance, R_{ct} - charge transfer resistance, R_{po} - pore resistance of the coating, C_c - coating capacitance, C_{dl} - double layer capacitance and Z_W is the Warburg element.

equivalent circuits in Figure 7b.

Chitosan-epoxysilane coated samples exhibited a higher impedance modulus than chitosan coated ones. As already shown by sputter depth profiling, the siloxane is bound directly to the metal surface, effectively passivating the zinc. Additionally, the phase shows an almost purely capacitive behaviour, especially when compared to the chitosan film. The higher impedance modulus of chitosan-epoxysilane film observed at high frequencies despite the use of the same electrolyte is attributed to an increased ionic resistance within the coat-

ing which can easily bind certain amounts of water and mobile ions. The high frequency modulus of the impedance is hence not only the resistance of the electrolyte, as typical for impedance spectra, but contains the ionic resistance of the coatings as well. In other words, the layer/electrolyte interface is "transparent" to a fraction of ions, which means that coating resistance contributes to the high frequency impedance.

Figure 8a shows the area-normalized capacitance of the intact polymer layer as function of time, calculated from fitting the EIS spectra at different times to the equivalent circuits in Figure 7b. The linear increase of the capacitance C_c of the intact chitosan film is expected for Fickian diffusion of water into the coating. This behaviour indicates free diffusion of water, with no effect of chemical interaction between the coating and the penetrating water.[54,66] The chitosan-epoxysilane coating showed a slower increase of the capacitance.

Comparing Figure 8, a and b, we observe that both the resistance and capacitance of the chitosan layer were increasing constantly with time. This constant increase of the resistance and capacitance suggests that the chitosan layer was dissolving and gradually exposing the substrate to the aqueous environment. Consequently, the ions approached the interface, which lead to formation of corrosion products blocking conductive paths. In addition, the remaining film continued to take up water. On the other hand, the resistance of chitosan-epoxysilane coating initially increased. The high resistance values are attributed to the presence of a thin SiO_2-like layer near the metal surface. Resistance is in the same order of magnitude as observed for chitosan-based coatings on aluminium alloys.[18,19] Resistance increase can be attributed to horizontal swelling of the dry coating that reduced the volume accessible to electrolyte solution. Furthermore, subsequent formation of corrosion products reduced the the available conduction paths even further. A drastic decrease of this resistance was observed after 120 min. Thereupon, resistance stabilizes and remained constant after long times, suggesting that the film does not suffer major degradation.

Moreover, the charge transfer resistance of chitosan-epoxysilane remained almost constant during the experiment. This constance can also be attributed to the presence of a non-degraded protective film. This results are in agreement with the LPR and SKP experiments, where the chitosan-epoxysilane hybrid possesses the highest inhibition of the corrosion current as well as showing the slowest delamination rate.

Furthermore, Figure 8c shows the volume fraction of water taken from the electrolyte calculated from C_c using Equation 3 for chitosan and chitosan-epoxsilane films. Because

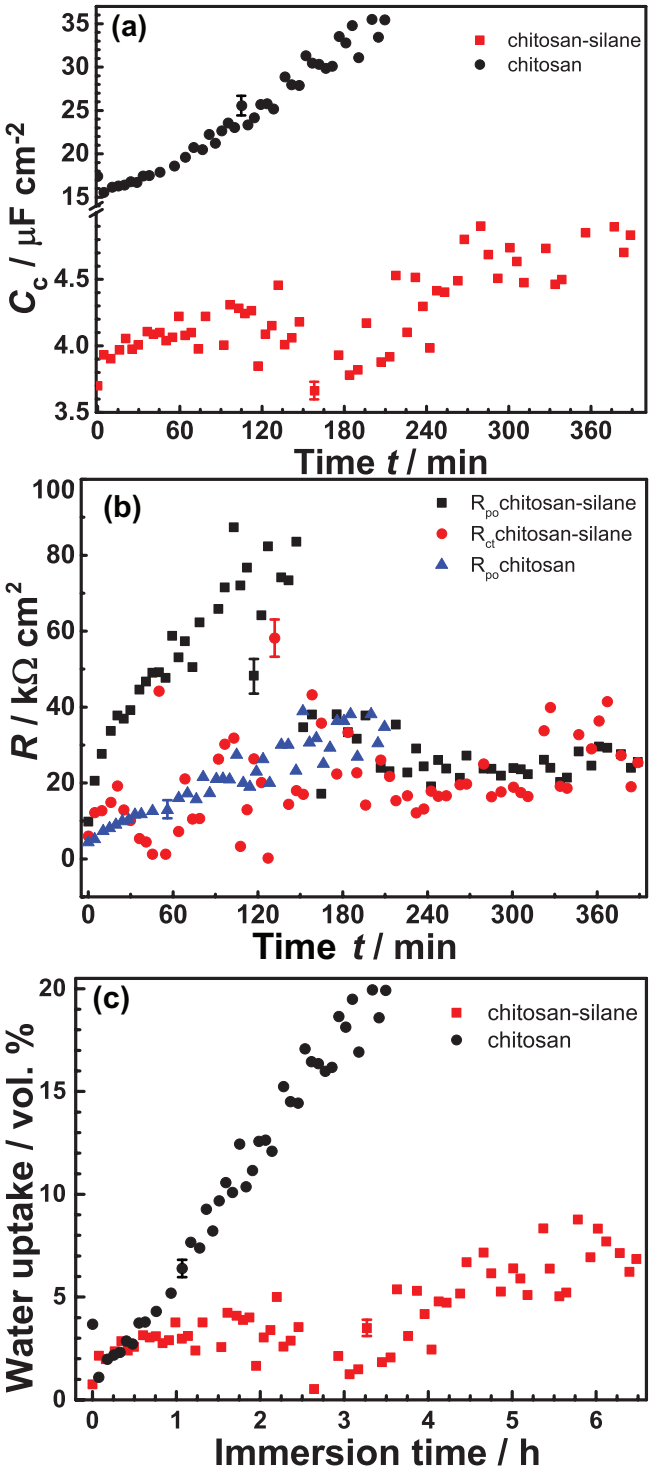

FIG. 8. (a) Capacitance of coatings in borate buffer, (b) resistance of chitosan and chitosan-epoxysilane coatings, and (c) water volume fraction calculated from C_c after exposure to borate buffer for different times. Representative error bars showing single standard deviation have been placed on individual data points of each series to keep the plots legible.

the coatings may take up water within several seconds after mounting the sample in the electrochemical cell, it is difficult to determine the exact swelling ratio from impedance measurements. However, water uptake on the chitosan-epoxysilane hybrid coating was much lower than for the chitosan coating only, and remained lower than 10 % during the whole experiment.

IV. SUMMARY AND CONCLUSIONS

Chitosan and a crosslinked derivative have been investigated as pretreatment-like protective layer against corrosion on the industrially important metallic zinc. A water-soluble epoxysilane coupling agent has been used to prepare chitosan-epoxysilane hybrid film with thickness in the order of 50-70 nm. This film formed a homogeneous layer on the metallic substrate, covering the complete substrate. The epoxysilane acts on the one hand as cross-linker within the coating, but also as linker to the oxide-covered zinc substrate.

Chitosan-epoxysilane hybrid coatings showed a larger resistance toward cathodic delamination and reduced oxygen reduction on the substrate compared to hydrophobic PVB, despite their water-solubility and their relatively fast water uptake. At low potentials above OCP, also the zinc dissolution is inhibited. A pure chitosan film showed a delamination rate reduced to 1/10 of that of a reference, while the added epoxsilane cross-linker lead to a further decrease in delamination rate to 1/3 of that of chitosan.

Chitosan-epoxysilane films exhibited a higher resistance to ion migration, as shown with EIS experiments and it possessed a much more stable and constant resistance than chitosan itself. The hydrophilicity of chitosan-epoxysilane hybrid films was significantly lower that its non-crosslinked version, as it was observed in the water uptake volume fraction. The SKP experiments show an offset in potential for the chitosan containing films, which is likely caused by the effect of a Donnan potential, indicating that the film is blocking selectively transport of one species of ions.

Films of this kind have hence the potential to slow down delamination in the long run by blocking the ionic current associated with cathodic delamination, even though they easily take up water. They may hence be used similar to conversion coatings as pretreatment.

ACKNOWLEDGEMENTS

This work was funded by the Initial Training Network Somatai, which is funded by the European Union's Seventh Framework Programme for research, technological development and demonstration under grant agreement no 316866. The authors thank Prof. M. Stratmann for continuous support, Michael Rohwerder for helpful discussions, and Petra Ebbinghaus as well as Adnan Sarfraz for technical support.

REFERENCES

[1]J. R. Davis, "Corrosion - understanding the basics," (ASM International, Materials Park, OH, USA, 2000) Chap. 1 - The Effects and Economic Impact of Corrosion, pp. 1–20.

[2]M. Stratmann, R. Feser, and A. Leng, Electrochim. Acta **39**, 1207 (1994).

[3]H. McMurray, A. Coleman, G. Williams, A. Afseth, and G. Scamans, J. Electrochem. Soc. **154**, C339 (2007).

[4]G. Grundmeier, C. Reinartz, M. Rohwerder, and M. Stratmann, Electrochim. Acta **43**, 165 (1998).

[5]G. Grundmeier and M. Stratmann, Annu. Rev. Mater. Res. **35**, 571 (2005).

[6]D. Zhu and W. J. Van Ooij, Prog. Org. Coat. **49**, 42 (2004).

[7]M. N. R. Kumar, React. Funct. Polym. **46**, 1 (2000).

[8]M. Teli and J. Sheikh, Int. J. Biol. Macromol. **50**, 1195 (2012).

[9]D. Sud, G. Mahajan, and M. Kaur, Bioresour. Technol. **99**, 6017 (2008).

[10]R. A. Cunha, E. F. Franca, F. J. Pontes, R. D. Lins, T. A. Soares, and V. H. Rusu, "The complex world of polysaccharides," (INTECH, Rijeka, Croatia, 2012) Chap. 9 - The molecular structure and conformational dynamics of chitosan polymers: an integrated perspective from experiments and computational simulations, pp. 229–256.

[11]S. Ifuku, M. Nogi, K. Abe, M. Yoshioka, M. Morimoto, H. Saimoto, and H. Yano, Biomacromolecules **10**, 1584 (2009).

[12]K. Kurita, Mar. Biotechnol. **8**, 203 (2006).

[13]A. Gandini, Green Chem. **13**, 1061 (2011).

[14]J. Synowiecki and N. A. A. Q. Al-Khateeb, Food Chem. **60**, 605 (1997).

[15]J. Synowiecki and N. A. Al-Khateeb, Crit. Rev. Food Sci. Nutr. **43**, 145 (2003).

[16]X. Pang and I. Zhitomirsky, Mater. Charact. **58**, 339 (2007).

[17]P. Dong, W. Hao, Y. Xia, G. Da, and T. Wang, J. Mater. Sci. Technol. **26**, 1027 (2010).

[18]J. Carneiro, J. Tedim, S. Fernandes, C. Freire, A. Silvestre, A. Gandini, M. Ferreira, and M. Zheludkevich, Prog. Org. Coat. **75**, 8 (2012).

[19]J. Carneiro, J. Tedim, S. Fernandes, C. Freire, A. Gandini, M. Ferreira, and M. Zheludkevich, Surf. Coat. Technol. **226**, 51 (2013).

[20]Z. Wei, C. Wang, S. Zou, H. Liu, and Z. Tong, Polymer **53**, 1229 (2012).

[21]Z.-G. Yue, W. Wei, P.-P. Lv, H. Yue, L.-Y. Wang, Z.-G. Su, and G.-H. Ma, Biomacromolecules **12**, 2440 (2011).

[22]P.-P. Lv, W. Wei, H. Yue, T.-Y. Yang, L.-Y. Wang, and G.-H. Ma, Biomacromolecules **12**, 4230 (2011).

[23]R. A. Muzzarelli and A. Isolati, Water, Air, Soil Pollut. **1**, 65 (1971).

[24]M. R. Kumar, R. Muzzarelli, C. Muzzarelli, H. Sashiwa, and A. Domb, Chem. Rev. **104**, 6017 (2004).

[25]E. Khor and L. Y. Lim, Biomaterials **24**, 2339 (2003).

[26]O. Lundvall, M. Gulppi, M. Paez, E. Gonzalez, J. Zagal, J. Pavez, and G. Thompson, Surf. Coat. Technol. **201**, 5973 (2007).

[27]Y. Shirosaki, K. Tsuru, S. Hayakawa, A. Osaka, M. A. Lopes, J. D. Santos, and M. H. Fernandes, Biomaterials **26**, 485 (2005).

[28]S. Spirk, G. Findenig, A. Doliska, V. E. Reichel, N. L. Swanson, R. Kargl, V. Ribitsch, and K. Stana-Kleinschek, Carbohydr. Polym. **93**, 285 (2013).

[29]D. Avnir, L. C. Klein, D. Levy, U. Schubert, and A. B. Wojcik, "Organo-silica sol–gel materials," in *PATAI'S Chemistry of Functional Groups* (Wiley, Hoboken, 2009).

[30]T. P. Braga, E. C. C. Gomes, A. F. de Sousa, N. L. V. Carreño, E. Longhinotti, and A. Valentini, J. Non-Cryst. Solids **355**, 860 (2009).

[31]J. H. Chen, Q. L. Liu, X. H. Zhang, and Q. G. Zhang, J. Membr. Sci. **292**, 125 (2007).

[32]S. Amado, M. Simoes, P. A. da Silva, A. Luís, Y. Shirosaki, M. Lopes, J. Santos, F. Fregnan, G. Gambarotta, and S. Raimondo, Biomaterials **29**, 4409 (2008).

[33]S. K. Yong, M. Shrivastava, P. Srivastava, A. Kunhikrishnan, and N. Bolan, in *Rev. Environ. Contam. Toxicol.*, Vol. 233, edited by M. D. Whitacre (Springer, Cham, Switzerland, 2015) pp. 1–43.

[34]K. Mittal, *Silanes and Other Coupling Agents* (VSP, Utrecht, The Netherlands, 1992).

[35]H. McMurray and G. Williams, in *Shreir's Corrosion*, edited by B. Cottis, M. Graham, R. Lindsay, S. Lyon, T. Richardson, D. Scantlebury, and H. Stott (Elsevier, Oxford, 2010) Chap. 2.14, pp. 988 – 1004.

[36]G. Grundmeier and S. Alda, "Encyclopedia of Electrochemistry," (Wiley-VCH, Weinheim, Germany, 2007) Chap. Corrosion Protection by Organic Coatings, pp. 500–566.

[37]A. Amirudin and D. Thierry, Prog. Org. Coat. **28**, 59 (1996).

[38]C. D. Fernández-Solis, A. Vimalanandan, A. Altin, J. S. Mondragón-Ochoa, K. Kreth, P. Keil, and A. Erbe, in *Soft Matter at Aqueous Interfaces*, Lect. Notes Phys., Vol. 917, edited by P. R. Lang and Y. Liu (Springer, Cham, Switzerland, 2016) pp. 29–70.

[39]H. Leidheiser Jr., W. Wang, and L. Igetoft, Prog. Org. Coat. **11**, 19 (1983).

[40]A. Leng, H. Streckel, and M. Stratmann, Corros. Sci. **41**, 547 (1998).

[41]W. Fürbeth and M. Stratmann, Corros. Sci. **43**, 207 (2001).

[42]D. Iqbal, J. Rechmann, A. Sarfraz, A. Altin, G. Genchev, and A. Erbe, ACS Appl. Mater. Interfaces **6**, 18112 (2014).

[43]R. Posner, M. Santa, and G. Grundmeier, J. Electrochem. Soc. **158**, C29 (2011).

[44]P. A. Sørensen, K. Dam-Johansen, C. Weinell, and S. Kiil, Prog. Org. Coat. **68**, 283 (2010).

[45]R. Montoya, F. García-Galván, A. Jiménez-Morales, and J. Galván, Corros. Sci. **82**, 432 (2014).

[46]D. Iqbal, A. Sarfraz, M. Stratmann, and A. Erbe, Chem. Commun. **51**, 16041 (2015).

[47]D. E. Azofeifa, H. J. Arguedas, and W. E. Vargas, Optical Materials **35**, 175 (2012).

[48]M. Stern and A. L. Geary, J. Electrochem. Soc. **104**, 56 (1957).

[49]L. J. C. Jeuken, "EISfit," http://www.fbs.leeds.ac.uk/jeukengroup/freeware/EISFit.php (accessed January 2016).

[50]G. Grundmeier, W. Schmidt, and M. Stratmann, Electrochim. Acta **45**, 2515 (2000).

[51]D. Brasher and A. Kingsbury, J. Appl. Chem. **4**, 62 (1954).

[52]H. Rosen and J. Martin, J. Coat. Technol. **63**, 85 (1991).

[53]G. Walter, Corros. Sci. **32**, 1041 (1991).

[54]E. Van Westing, G. Ferrari, and J. De Wit, Corros. Sci. **36**, 957 (1994).

[55]E. Barsoukov and J. R. Macdonald, *Impedance spectroscopy: theory, experiment, and applications* (Wiley, Hoboken, 2005).

[56]Y.-L. Liu, Y.-H. Su, and J.-Y. Lai, Polymer **45**, 6831 (2004).

[57]J. D. Minford, *Handbook of aluminum bonding technology and data* (CRC Press, Boca Raton, FL, USA, 1993).

[58]R. A. Nyquist, *Interpreting infrared, Raman, and nuclear magnetic resonance spectra* (Academic Press, San Diego, CA, USA, 2001).

[59]J. Coates, "Interpretation of infrared spectra, a practical approach," in *Encyclopedia of Analytical Chemistry* (Wiley, Chichester, UK, 2000).

[60]B. C. Trasferetti, C. U. Davanzo, and M. A. Bica de Moraes, J. Phys. Chem. B **107**, 10699 (2003).

[61]"XPS Knowledge Base," http://xpssimplified.com/ (accessed December 2015).

[62]R. Benoit, Y. Durand, B. Narjoux, and G. Quintana, http://www.lasurface.com/ (accessed December 2015).

[63]A. Leng, H. Streckel, and M. Stratmann, Corros. Sci. **41**, 579 (1998).

[64]M. Beppu, R. Vieira, C. Aimoli, and C. Santana, J. Membr. Sci. **301**, 126 (2007).

[65]A. Bard and L. Faulkner, *Electrochemical methods: Fundamentals and applications* (Wiley, New York, 2001).

[66]E. Van Westing, G. Ferrari, and J. De Wit, Corros. Sci. **34**, 1511 (1993).